Advanced Concept for Air Data System using EBF and Lidar

A.K. Mohamed, J. Bonnet

ONERA – Physics, Instrumentation and Sensing Department, Chemin de la Hunière, 91761 Palaiseau, France

Ajmal_Khan.Mohamed@onera.fr

ABSTRACT

We describe here two innovative in-flight measurement techniques for onboard operation on atmospheric re-entry demonstrator vehicles like EXPERT or pre-X actually in study in Europe. The first one is the Electron Beam Fluorescence (EBF) technique which aims at characterising shock layer chemistry through measurements of density, rotational and vibrational temperatures of N_2 and NO in low density hypersonic flows. These data are of great importance for the validation of the modelling tools commonly used for aerothermodynamics simulations, since they include a variety of thermo-chemical models yet to be fully validated with relevant flight data. The second measurement technique is a short range Rayleigh Lidar for measurements of upstream total density which is a primary variable in many aerodynamic key features like forces or heat flux.

1   Introduction

On a vehicle, classical measurement means as temperature gauges or pressure taps usually only give access to wall quantities. Physical phenomena that occur at the wall nevertheless depend on what happened earlier inside the flow field, in particular for hypersonic flows through the nose shock of the vehicle. Understanding and accurate prediction of what happens at the wall therefore imply the same

quality of understanding and modelling of the upwind flow field, that means also good characterisation with suitable diagnostics. In addition for high enthalpy flows, chemistry and non equilibrium phenomena are of primary interest and require advanced diagnostics in order to be properly characterised in terms of velocity, translational, rotational and vibrational temperatures profiles within the flow field. Such diagnostics have been developed for ground facilities (Figure 1), but ground to flight extrapolation, which remains a challenge for hypersonics, justify considering the use of such diagnostics in flight experimentation to enrich the experimental flight database.

But flight extrapolation brings other stringent conditions, the first one being that the detection system must also be on the vehicle. This condition thereby selects only techniques enabling backscattered photons like laser or electron beam induced fluorescence and Rayleigh or Raman scattering. Other factors like complexity and sensitivity for N_2, the principal specie to be investigated, further reduce the choice, with present technology, to only a few techniques. In this paper we will describe only two of these, namely Electron beam fluorescence and Rayleigh scattering.
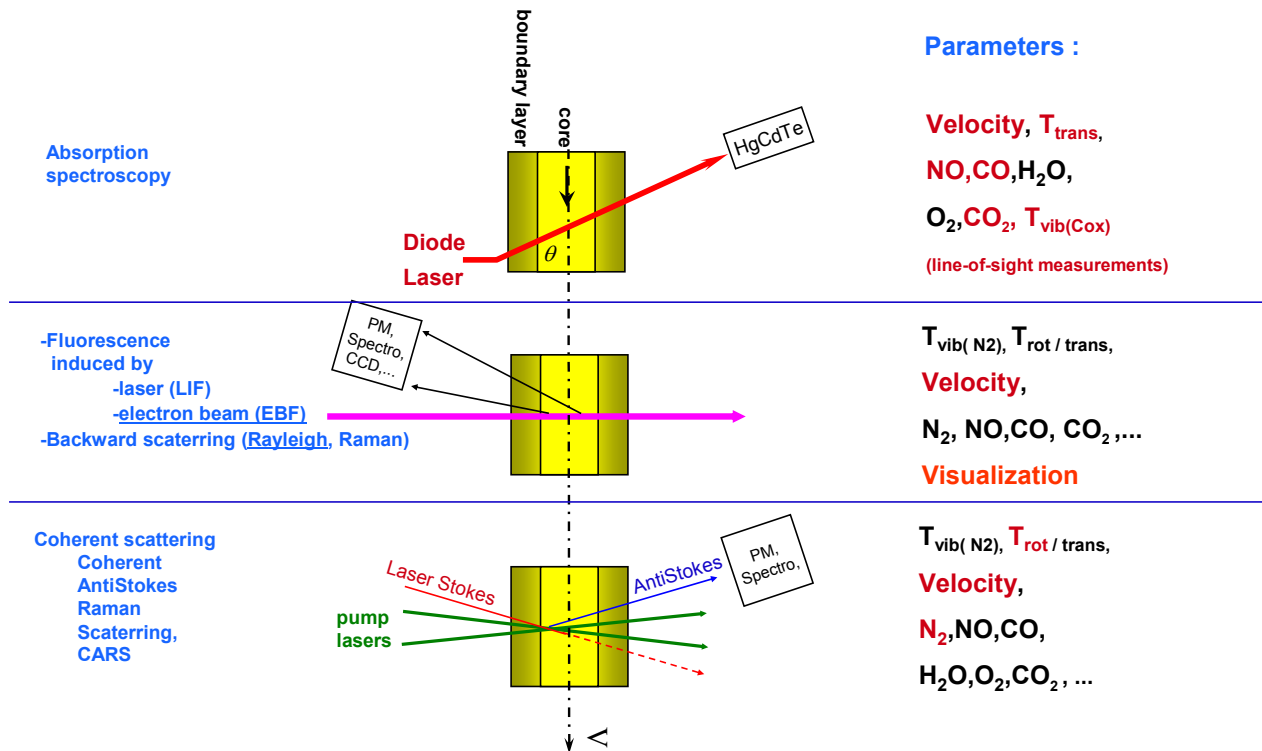
Figure 1 – Some optical diagnostics techniques (non-intrusive) applied in wind tunnels

2   The Electron Beam Fluorescence Technique (EBF)

2.1   Overview

The Electron beam fluorescence (EBF) technique is a well established tool to perform local and non intrusive measurements of density, vibrational and rotational temperatures and velocity in low density hypersonic flows ($< 10^{16}$ molecules/cm^3) on different species like N_2, NO, CO, CO_2 and He ([1] to [8]). The technique has also been used on several occasions for in-flight measurements on board rockets to probe the shock layer or the upper atmosphere ([12] to [15]). Reference [7] is an excellent long review of the technique.

The EBF technique is based on the excitation (and related broadband fluorescence) induced by an electron beam on the gas atoms and molecules along the electron beam path. Figure 2 presents a typical setup of EBF in a wind tunnel application. In a low density gas flow, the use of an energetic electron beam (typically 25 keV) induces a complicated set of excitations in the gas all along the beam. These excitations produce broadband fluorescence ranging from X ray to the infrared. Each molecular or atomic specie has its characteristic EBF signature in the form of characteristic vibrational bands or rotational emission lines from which measurements specific to that specie can be performed.
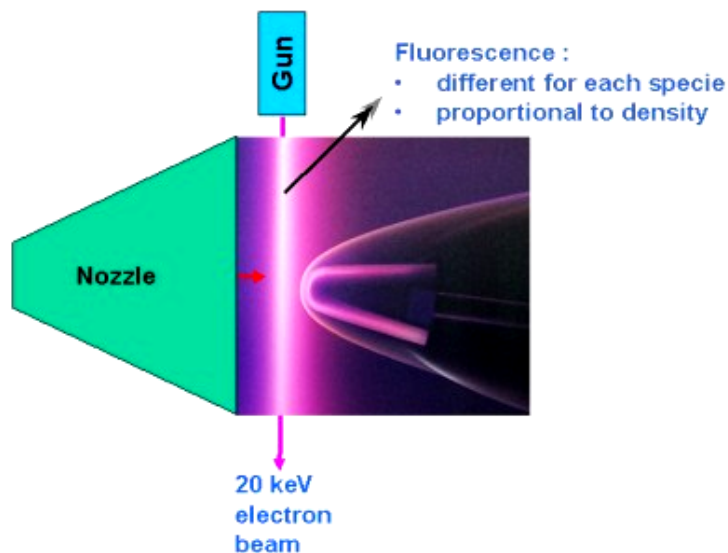
Figure 2 - Typical setup of EBF in a windtunnel - Visualisation of the electron beam and exploitation of its afterglow to visualise a Mach 10 flow around the ESA EXPERT atmospheric reentry vehicle

For molecular Nitrogen, the main emissions in the UV and visible spectrum (Figure 3) are mainly the first negative system N_2^+(1N) and the second positive system N_2(2P) from which most of the measurements are performed. For NO, the most prominent bands are the gamma bands in the UV between 200 and 300 nm.
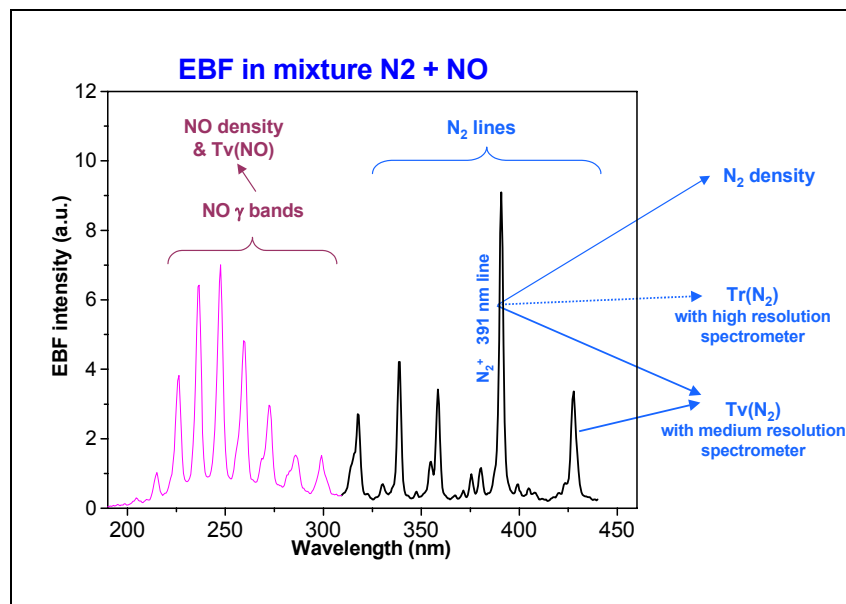
Figure 3: EBF spectra of N_2 and NO

For a given specie, the spectral analysis of its fluorescence provides the vibrational temperature and even the rotational temperature if high spectral resolution can be afforded for that specie. The density of that specie in the flow can be measured from the intensity of one or a few of its fluorescence lines. Velocity measurements can also be performed through Doppler shift of the radiative emission or by a time of flight method [2][3].

The measurements can be useful in the following applications:

- Validation of aerodynamic simulation codes from wind-tunnel or in-flight testing
- Gas-surface accommodation
- Atmospheres of other planets

Table 1 presents the different parameters which can be measured on nitrogen based flows.

Parameter	Range
Flow Density	10^{13} -10^{16} molecules/cm^3
Flow visualization	10^{13} -10^{17} molecules/cm^3
Temperatures - of rotation Tr - of vibration Tv	as from a few Kelvins > 1000 K
Velocity (Doppler or Time of flight)	> 1000 m/s

Table 1 - Parameters which can be measured by EBF on nitrogen based flows

The measurements are:

- non-intrusive
- local (spatial resolution depends mainly on the optical imaging of the fluorescence from the beam which has usually a diameter of 1 mm : we can have easily a resolution of 1 mm3)

The technique has also been used on other species like NO, O_2, O and N mainly to study gas discharges and in Helium flows for high Mach numbers studies. Actually, there is a renewal of interest in extending the technique to higher densities and to probe CO/CO2 flows (Mars atmosphere studies).

2.2   Measurement principle

Electron impacts on atoms or molecules induce transitions among the energy levels of the atoms or molecules as depicted in Figure 4. The interactions follow dipolar rules for electrons of energy higher than 800V. For lower energies, quadrupolar excitations become quite important and provide higher fluorescence rates but these are difficult to exploit because of too high non-linearity between the fluorescence intensity and electron beam intensity or gas number density. For this reason and also for sufficient propagation of the beam in a low density gas, the technique is usually applied with electron energies of a few keV. It is then comparable to laser induced fluorescence (LIF): from knowledge of the radiative emission and excitation coefficients one trace the intensity of a fluorescence line to the population number density of a fundamental energy level. In fact, in EBF there is broadband excitation of many fundamental levels due to the high energy of the electrons thereby allowing to measure population distributions on many fundamental levels simultaneously.
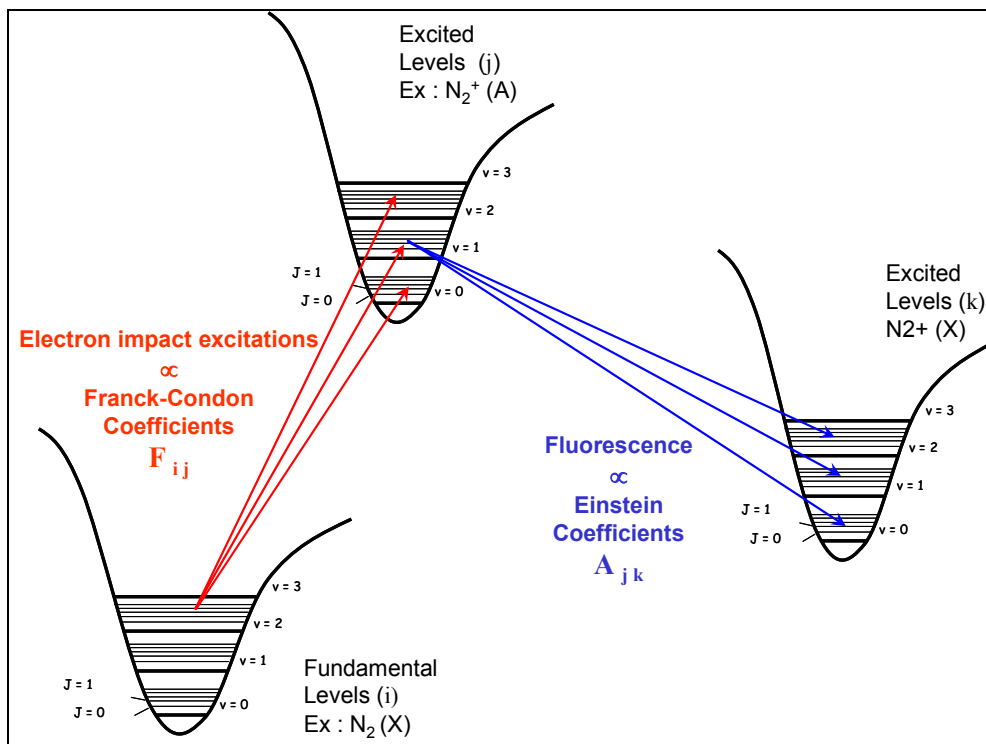
Figure 4 - Electron Beam excitation-fluorescence principle

Using the notations of Figure 4, the population change rate of level j from electron impact excitation from level i is given by:

$$\frac{dn_{j|i}}{dt}\bigg|_e = n_p\, v_p\, \sigma_{ij}(E_p)\, n_i \qquad \textbf{E 1}$$

n_i, n_j : populations on levels i,j; both are proportional to the total density n_0 of the gas
n_p : density of primary electrons
v_p : velocity of primary electrons
E_p : energy of primary electrons, $E_p = \frac{1}{2}\, m_e v_p^2$, m_e being the electron mass
$\sigma_{ij}(E_p)$: cross section of the excitation by electron impact.

For dipolar excitations, the cross-section has the following dependency on the electron energy E_p :

$$\sigma_{ij} = \alpha_{ij}\frac{\ln(\beta_{ij}E_p/E_{ij})}{E_p/E_{ij}} \qquad \textbf{E 2}$$

where

α_{ij} and β_{ij} are coefficients specific to a specie and to the energy levels considered (usually deduced from experiments),

$E_{ij} = |E_j - E_i|$ energy difference between levels i and j.

As an example, we report here from reference [9] the dipole excitation cross section equation the transition $N_2X^1\Sigma_g^+(v''=0) \rightarrow N_2^+B^2\Sigma_u^+(v'=0)$, which contributes to the N_2 most prominent line ($N_2^+1N(0,0)$ at 391.4 nm):

$$\sigma_{00} = 1585\frac{\ln(E_p/22)}{E_p}10^{-18}\ \ cm^2 \qquad \textbf{E 3}$$

with E_p in eV valid for energies higher than 200 V.

The change in population of the same level j due to radiative emission to level k is expressed as :

$$\frac{dn_{j|k}}{dt}\bigg|_v = n_j\, A_{jk} \qquad \textbf{E 4}$$

where A_{jk} is the probability of radiative transition in s^{-1}. The intensity of this radiative emission between levels j and k is

$$I_{jk} = n_j\, A_{jk}\, h\, \nu_{jk} \qquad \textbf{E 5}$$

where   h   : Planck constant
ν_{jk} : frequency of the transition j-k

If we neglect other mechanisms for population change on level j, then

$$\frac{dn_j}{dt} = \sum_i n_p\, v_p\, \sigma_{ij}(E_p)\, n_i - \sum_s n_j A_{js}$$
$$= 0 \quad \text{at stationary state}$$

E 6

The intensity of a fluorescence line is then :

$$I_{jk} = n_j A_{jk} h\nu_{jk} = h\nu_{jk}\, \frac{\sum_i n_p\, v_p\, \sigma_{ij}(E_p)\, n_i}{\sum_s A_{js}/A_{jk}} \quad \propto \quad n_0$$

E 7

and therefore is proportional to the total density of the gas n_0 as n_i is proportional to n_0.

This linear dependence is valid up to density levels of 10^{16} cm^{-3}. Above that value there are two phenomena which cause deviations from linearity :

- Fluorescence quenching (collisional non radiative de-excitation)

- Supplementary excitations by secondary electrons (created through ionisation from the electrons of the beam and which have sufficient energy to bring excitations (quadrupolar mainly).

Beam dispersion becomes important also as from 10^{16} cm-3.

Secondary effects	Criteria	Upper density limit n_g in molecules.cm^{-3}
Beam dispersion	Beam propagation length for at least 100 mm	$\leq 10^{16}$
Quenching	Linear relation between intensity of fluorescence and gas density: $I = \alpha n_g$	$\leq 3.10^{16}$
Secondary electrons	Excitations by e_s are less than excitations by e_p	$\leq 10^{16}$

Table 2 – Main causes for EBF limitation to low densities

2.3 Measurements examples

Figure 5 recalls the typical setup in a wind tunnel as well as the potential measurements of the EBF technique matched against the appropriate optical detectors.
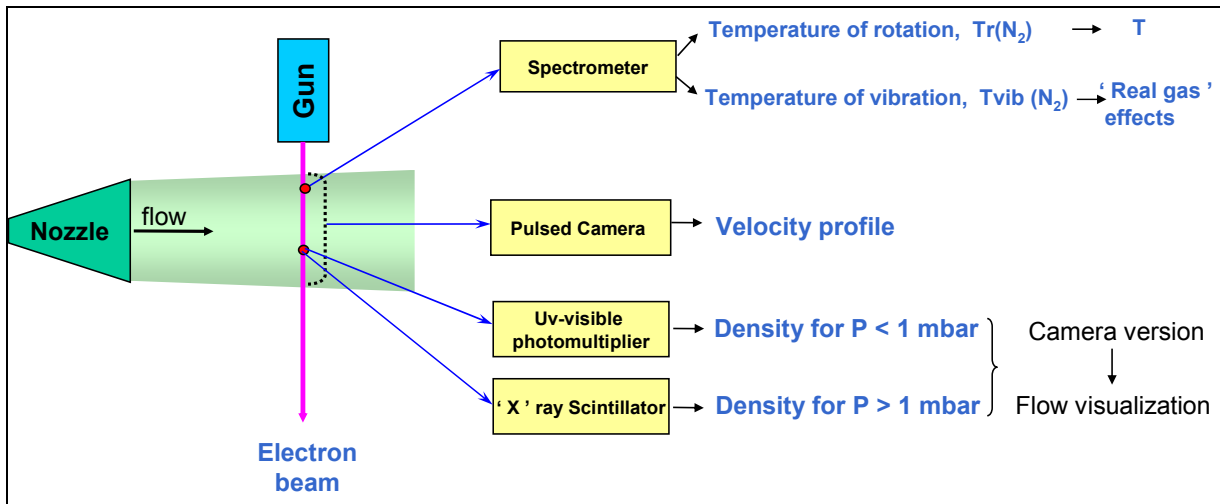
Figure 5- EBF potential measurements and setups in windtunnels

2.3.1 Density and flow visualisation

Density measurements are quite straightforward in a low density gas (up to 10^{15} molecules/cm^3) where the intensity of fluorescence is directly proportional to the density as shown in paragraph 2.2. As mentioned above, for higher densities collisional non radiative de-excitation (quenching) sets a non-linear relationship between fluorescence intensity and density, where other parameters like temperature are involved. Nevertheless, qualitative density variation can still be useful to assess better understanding of flow structure, pointing out for instance shock waves. This is usually done by sweeping the beam to illuminate a sheet of the flow, which provides spectacular images of visualisation.

Figure 6 shows an example of interaction of shock waves between two models placed in a Mach 10 flow (ONERA R5 wind tunnel). Densities are here too high ($> 10^{16}$ molecules/cm^3) to allow accurate density mesurements by using visible fluorescence, but this kind of visualisation can help to configure the models and to choose the right type of interaction for more accurate measurements by other techniques (CARS for instance).
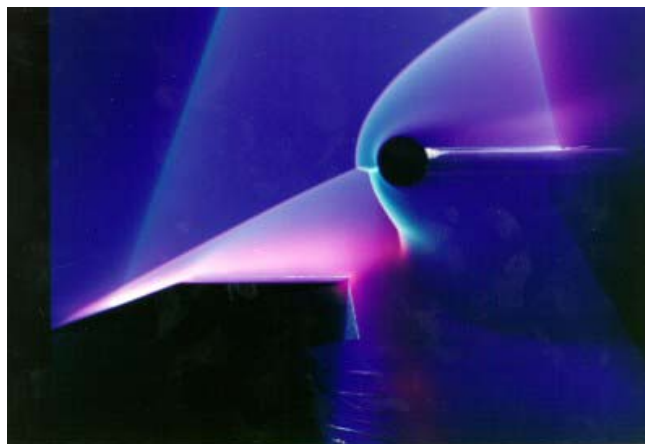
Figure 6 – EBF visualisation of interaction of shock waves in a Mach 10 flow

The following pictures show flow visualisation around some other models which have been studied in the ONERA R5 wind Tunnel.

Figure 7 - Mars sample Return Orbiter in aero capture phase
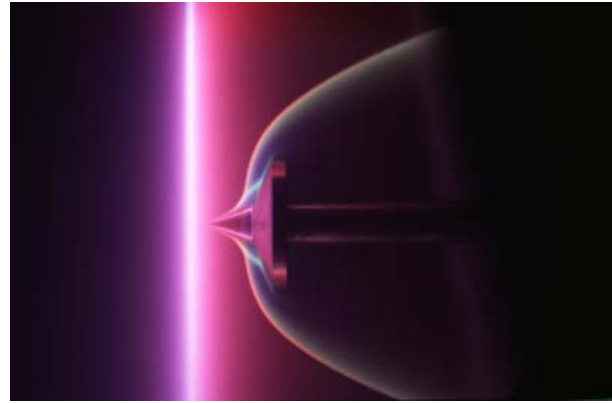
Figure 8 - Double cone for SWBLI studies
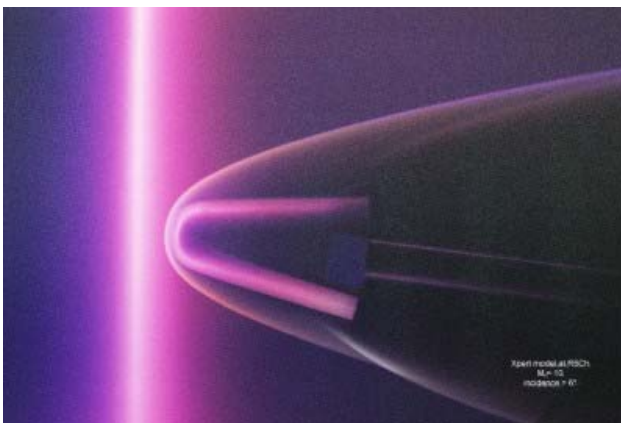
Figure 9 - ESA EXPERT ballistic re-entry model for basic re-entry studies
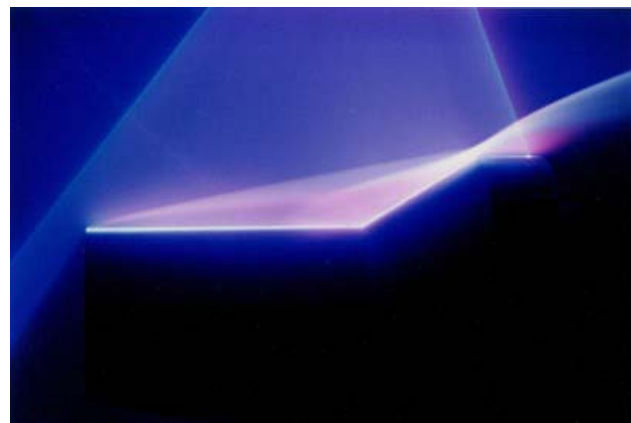
Figure 10 - *Holow cylinder for SWBLI studies*

2.3.1.1   *Density measurements using X ray radiation*

For quantitative point measurement of density at higher values than 10^{16} molecules/cm^3 , X-ray emission, composed of Bremsstrahlung and characteristic radiation, is preferable because it is not subject to quenching and to spectral broadening (both depend on temperature and pressure and introduce non-linearity in the response). In principle, there are thus no physical limitations to employing this approach, provided the spatial resolution is much less than the electron mean free path. We present here a result of X-ray technique set to examine the air flow structure near a model (hollow cylinder with a ramp) specially designed for shock wave / boundary layer interaction studies. To avoid interference of strong X-ray radiation scattered from the model surface, the electron beam is passed through a tube inserted into the model and cut flush at the model surface. The density measurements can then be made down to 2 mm from the surface. Figure 11 compares the experimental density profile obtained at position X/L = 0.76 to

results obtained from DSMC and Navier-Stokes calculations.
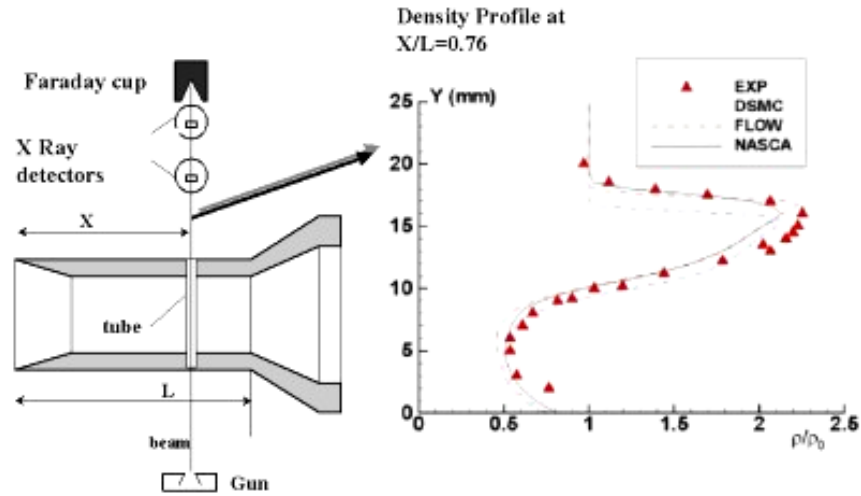
Figure 11 - EBF density profile measurements and comparison to CFD

2.3.2   Vibrational temperature

For temperature measurements, we need to further develop the notations in §2.2 to take into account the different features contributing to a molecular state and identifying it. We use standard molecular notations for the quantum numbers associated to each movement contributing to the internal energy of a molecular state :

- Motion of the electronic cloud (Λ)
- Vibration of the atoms constituting the molecule (v)
- Rotation (J)

Assuming independence between these movements, one can assign a temperature to each of them, keeping in mind that thermodynamic equilibrium occurs only when all these temperature are equal. Using customary molecular notations, the population on a molecular energy level can therefore be written as

$$ n_{\Lambda vK} = n_0 \cdot \frac{e^{-\frac{E_\Lambda}{kT_\Lambda}}}{Q_{elec}} \cdot \frac{e^{-\frac{E_v}{kT_V}}}{Q_{vib}} \cdot \frac{e^{-\frac{E_J}{kT_R}}}{Q_{rot}} \qquad \textbf{E 8} $$

where k is the Boltzmann constant and Q the partition function.

The intensity of fluorescence of a rotational line, rearranging E5 and using E6, is written as

$$ I_{\Lambda''v''J''}^{\Lambda'v'J'} = \frac{q_{v'v''} P_{J'J''} R_{\Lambda\Lambda'}}{2J'+1} \sum_{vJ} n_{\Lambda vJ}\, q_{v'v}\, P_{J'J} \qquad \textbf{E 9} $$

where the excitation cross section coefficient matrix element is

$$R_{\Lambda\Lambda'} = n_p \, v_p \, \sigma_{\Lambda\Lambda'}(E_p) \qquad \textbf{E 10}$$

neglecting secondary electrons effects and where

- $q_{v'v''}$ = Franck-Condon factors coupling vibrational levels,

- $P_{J'J''}$ are Holn-London factors for coupling rotational levels.

If we limit ourselves to vibration levels on only the fundamental electronic level (Λ=0 which usually the case in our applications), and sum on all rotational elements in E9, we have the following expression for a vibrational line :

$$I_{v'v''} = q_{v'v''} \, R_{\Lambda\Lambda'} \sum_v n_v \, q_{v'v} \qquad \textbf{E 11}$$

Usually, most of the populations are on the first few vibrational levels of the molecule even at high vibrational temperatures (~3000 K). Measuring the corresponding fluorescence lines (Figure 12) and inverting equation E 11 will determine a set of n_v from which the vibrational temperature T_V can then be obtained from the correspondence $n_v = n_0 e^{-(E_v/KT_V)}$.
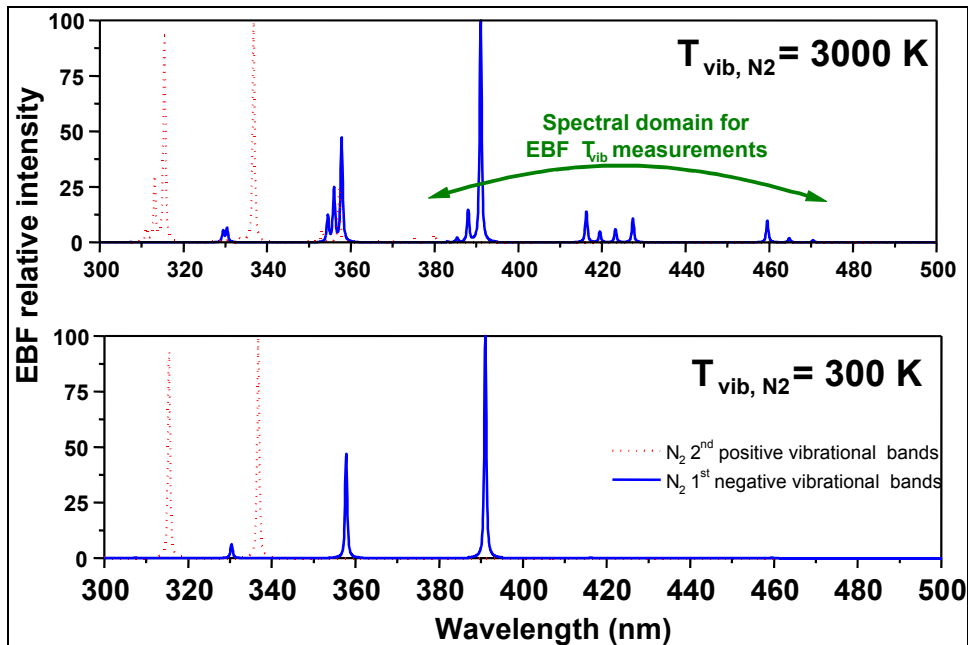
Figure 12: Illustration of N2 spectral emission difference for two gas vibrational temperature

2.3.3   Rotational temperature

Nitrogen rotational temperature measurement is another important possibility of electron beam fluorescence technique. A high resolution spectrometer must be used to resolve the rotational structure of one of the vibrational bands of nitrogen. The rotational temperature can be derived using the same procedure as for vibrational temperature determination described above.

The vibrational 0-0 band emitted near 391.4 nm is usually chosen as it is the most intense band at low density. Different excitation-desexcitation models [1,2,9] have been built to extract the rotational temperature from the relative intensities of the rotational lines of both the P and the R branches composing this band. When the spectral resolution is not sufficient to separate completely the lines, synthetic spectra must be built to be compared with the experimental spectrum. Usually a non-linear least square fit procedure is used to find the simulated spectrum which best matches the experimental one.

To illustrate rotational temperature measurement capability, we present here an application which enabled to characterise a gas containing two group of molecules each having a different rotational temperature (transient phase). The application aimed at measuring the rotational temperature of nitrogen molecules reflected from a 5 mm diameter disc placed in a hypersonic flow.

The experiments were carried out in cooperation with the DLR at the V2G wind tunnel in Göttingen [10][11]. The Knudsen number is set to be very high (low density flow and small surface) in order to prevent any shock wave to be formed in front of the surface : the molecules are just reflected from the surface. Measuring the rotational temperature of these reflected molecules allow to study how these molecules accommodate with the temperature of the surface which can be varied from room temperature up to 1200 K. The effect of the velocity of the incoming molecules has also been studied through variation of the stagnation temperature of the flow 300 K to 1200 K .

The beam is set to cross the flow vertically at a distance of 1 mm from the disc surface. A simple lens conjugates about 1 mm of the beam on the entrance slit of a high resolution spectrometer. Figure 13 shows spectra acquired in 100 seconds and which have sufficient spectral resolution to discern rotational features. Figure 13 a shows the rotational spectrum of only the free flow when the model is away. The rotational temperature in this case is 32 K for the stagnation conditions of 1020 K and 5 bar. In front of the disc surface, the rotational structure of the fluorescence (Figure 13.b and c) is more complex as it is a superposition of fluorescence from two group of molecules : the free flow molecules and those reflected from the surface (here found to be at 1000 K. The density of the reflected molecules can also be deduced from spectrum inversion : it is here seen to be about three times higher than the free flow one in the probe volume. All data interpretation is given in [11].
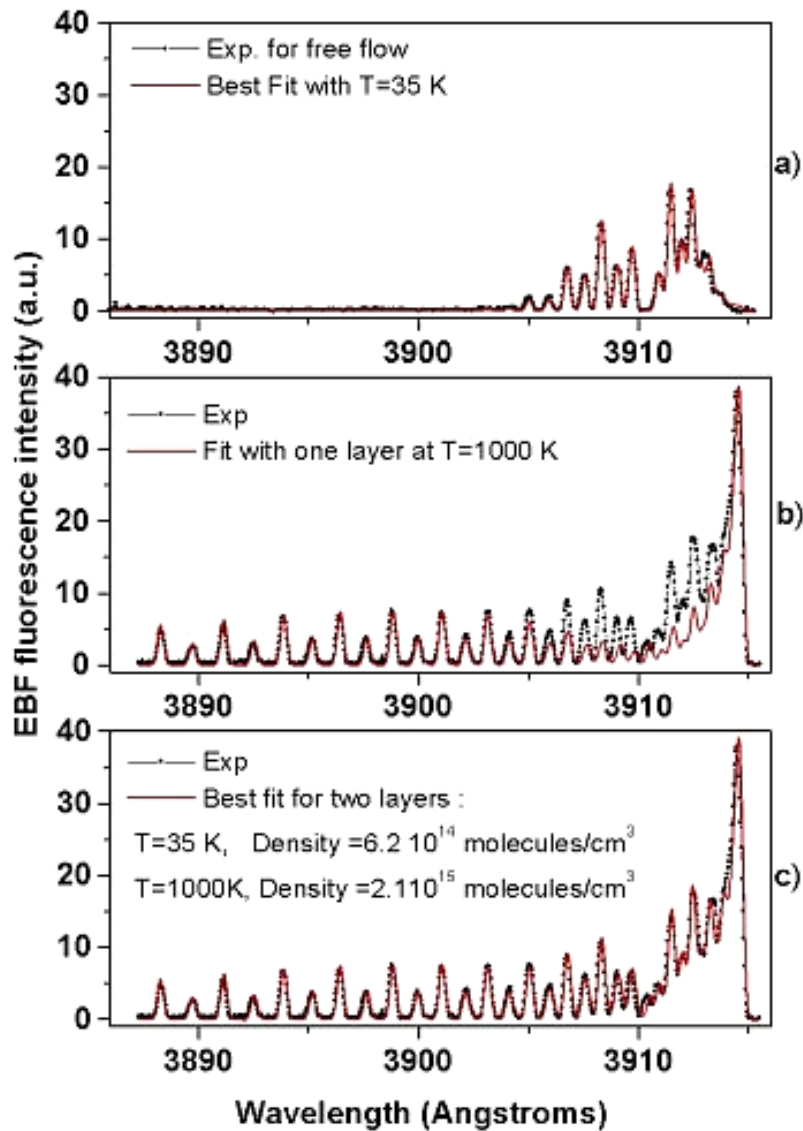
Figure 13 – Rotational spectra for N₂

2.3.4   Velocity

Velocity measurements by EBF can be performed using the following methods:

- Doppler shift technique

- Time of flight technique

   o   Electrical detection with Langmuir probes

   o   Optical detection of afterglow

The Doppler shift technique is quite straightforward by simply analysing the Doppler shift induced in the

fluorescence lines observed by a high resolution spectrometer at an angle which is the smallest possible to the flow axis [2]. We will here describe more thoroughly the time of flight method and particularly the one with optical detection of afterglow.

2.3.4.1 *Velocity Measurements using a classical pulsed electron beam*

Gas ionization is an important process among the excitations due to the electron beam. This phenomenon can be exploited, by pulsing the electron beam, to induce columns of plasma which are convected by the flow. The plasma columns contain mainly N_2^+ ions and low energy secondary electrons e_s produced during the ionization process.

After tagging the flow with these columns of plasma, local velocity measurements can be done by measuring the time of flight of the plasma columns between two chosen points through electrical detection of the N_2^+ ions (or the secondary electrons) with Langmuir probes[3].

The movement of the plasma columns can also be traced by the radiative emissions (afterglow) produced from secondary electron excitations in the columns. Some of the secondary electrons have sufficient energy to excite molecules of the gas producing fluorescence (N_2^+1N and $N_2 2P$ emissions) similar to the one due to excitations by the primary electrons of the beam. These secondary excitations can occur over a relatively long distance downstream from the electron beam, depending of the flow velocity and the relaxation time of the secondary electrons. The radiative lifetime τ of the excited molecules is very short ($\tau \sim 60$ ns), which means that the fluorescence can be considered to be emitted at the point of excitation in the columns for flow velocity V less than 10000 m/s.

Velocity measurements can be done here by measuring the distance of flight of the luminous plasma columns during a known time interval. For a single column, a streak and/or intensified camera for example can be used to perform snapshot pictures at different known times to follow the column displacement. The opening time must be very short (of the same order of the radiative lifetime) to freeze the movement of the column at each opening. Usually, the light collected is quite low and one must use image accumulation to enhance detection if the flow velocity is constant. A further improvement is to use a train of columns induced at regular intervals of time by a pulsed electron beam and perform stroboscopic detection by a camera whose openings are pulsed at the same frequency of the electron gun. The use of chemiluminescent reactions of $N_2(A)$ metastables (created by the electron beam) with species like NO or OH can also be used to enhance optical detection of the plasma columns[6].

Figure 14 presents an image of acceptable contrast for measuring the free stream velocity in the Mach 10 flow using a frequency of 100 kHz for both electron gun and camera pulses. The application inside a shock layer is more difficult as knowledge of the local direction of the velocity or the stream lines structure must first be known.
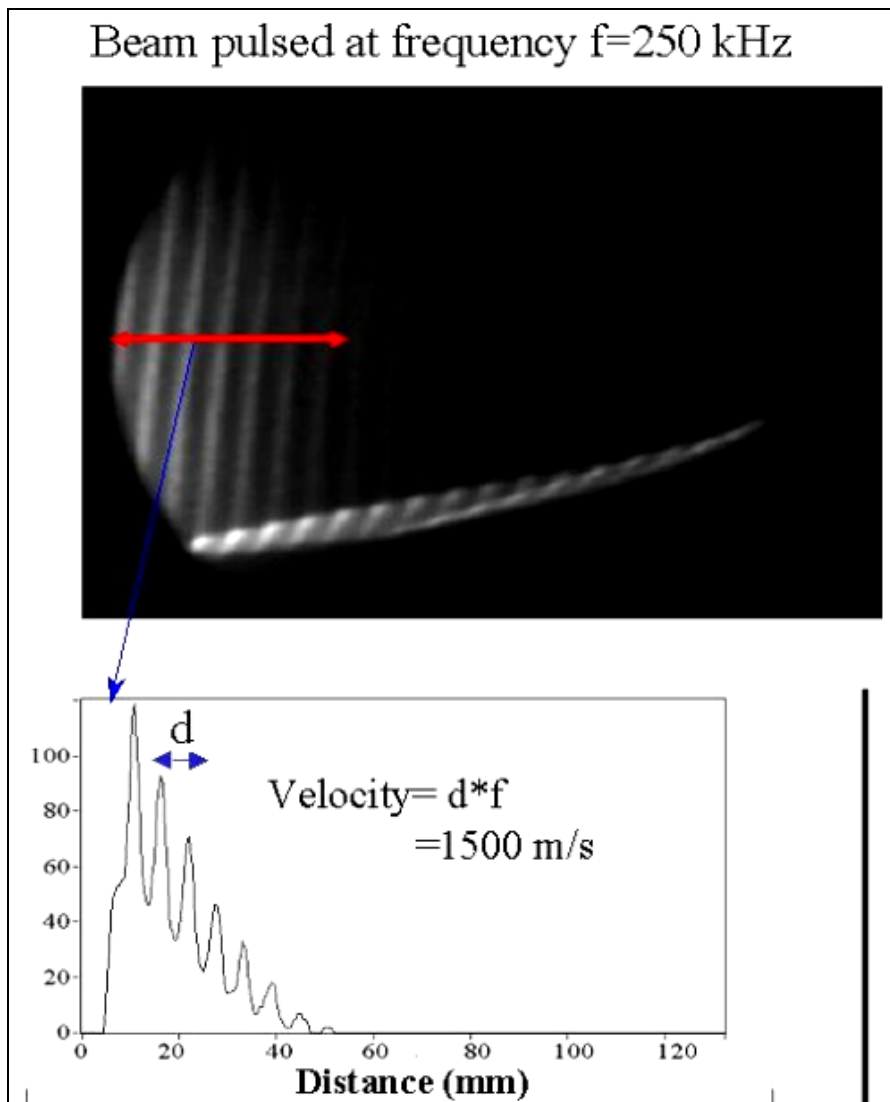
Figure 14 – Velocity measurements using pulsed afterglow

2.3.4.2 *Velocity Measurements Across The Boundary Layer in Hypersonic Flows Using a Pseudospark Electron-Beam-Assisted Glow Discharge*

Instead of image accumulation, one can try to increase the afterglow by using a more intense electron beam or some technique to increase the number of excitations in the plasma column. One such method is to use a pseudospark type electron gun which by principle of operation delivers a pulsed beam of some tens of nanoseconds. However, the high current intensity (a few amperes) remains insufficient to perform single shot detection with an intensified CCD. One way to further increase the afterglow is to create and maintain a glow discharge in the plasma column created by the pseudospark beam through proper electrical ground connections [8].

This pseudospark technique has the further advantage to be quite small in dimensions so that it can be placed inside a model to measure velocity profile in a shock layer of simple geometry. We present in the following, an example of velocity profile across a boundary layer obtained with an electron gun inside a

model in the Mach 10 R5 low-density, hypersonic, wind tunnel at ONERA. In these experiments, an intense pulsed electron beam is emitted by a very small (2cm x 3 cm) pseudo-spark [16][17] electron gun located inside the model (2D grounded metallic plate). It penetrates the flow from a 0.3 mm hole across the surface, and traces the path of a high voltage glow discharge in some ten nanoseconds. The filamentary discharge is instantaneously connected to a high voltage capacitor via a thin high voltage metallic rod placed, parallel to the flow axis, 100 mm away from the gun exit. This maintains the gaseous filament very bright during some microseconds. The initial linear pattern of the discharge then closely follows the streamlines which are known in this case. One verifies that no distortion occurs when the discharge is triggered within the same gas at static pressure.

At a precise delay time (5 µs) after the electron gun actuation, a CCD camera is opened briefly (250 ns) to image the position of the luminous column convected by the flow (Figure 15). The local velocity of the stream versus the distance above the plane is simply deduced from the horizontal displacement of a given point during the selected delay time.
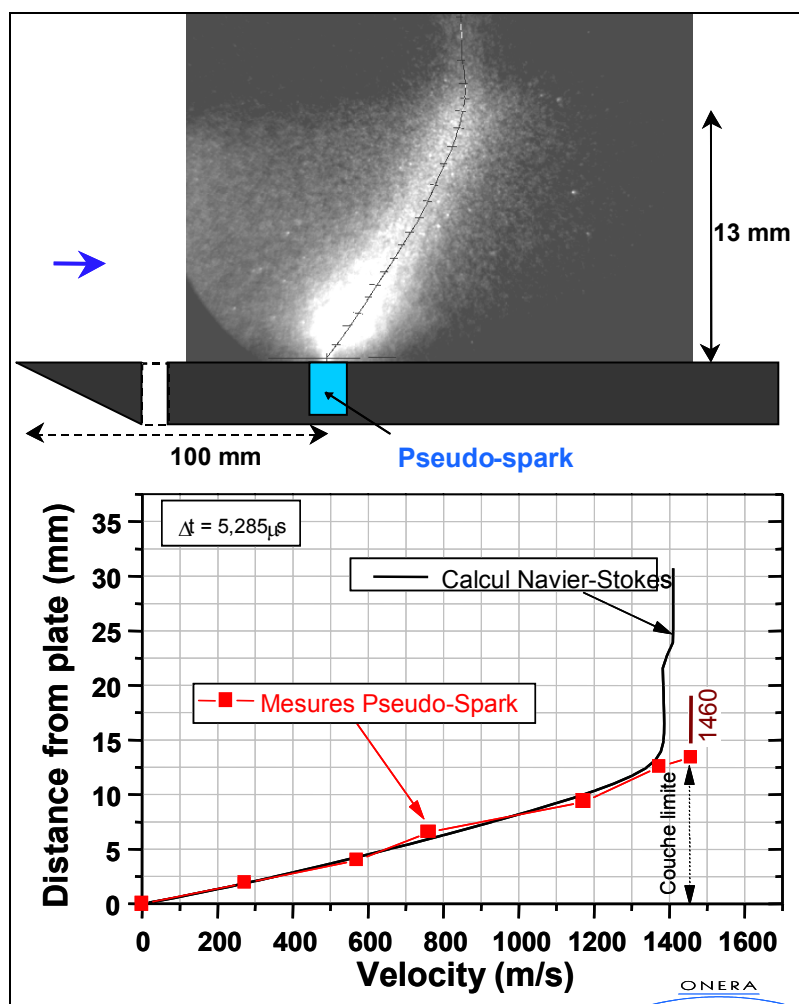
Figure 15 – Velocity profile measured by a pseudospark electron from within a flat plate model in the ONERA R5 Mach 10 wind tunnel

The observation field extends two cm above the model. As a calibrated grid is used to determine the

magnification of the optics, the global accuracy of this method can be estimated to 50-100 m/s. For identical aerodynamic conditions, the measured velocity profile compares correctly to the results of a numerical Navier-Stokes calculation.

2.4   Electron guns

Electron gun is a key element in the EBF technique. There are mainly three types of guns:

- filament-heated [1][2][3],
- secondary emission (beam or sheet)[4],
- pseudo spark [8][16][17],

and their main characteristics are presented in Figure 16 and Table 3.
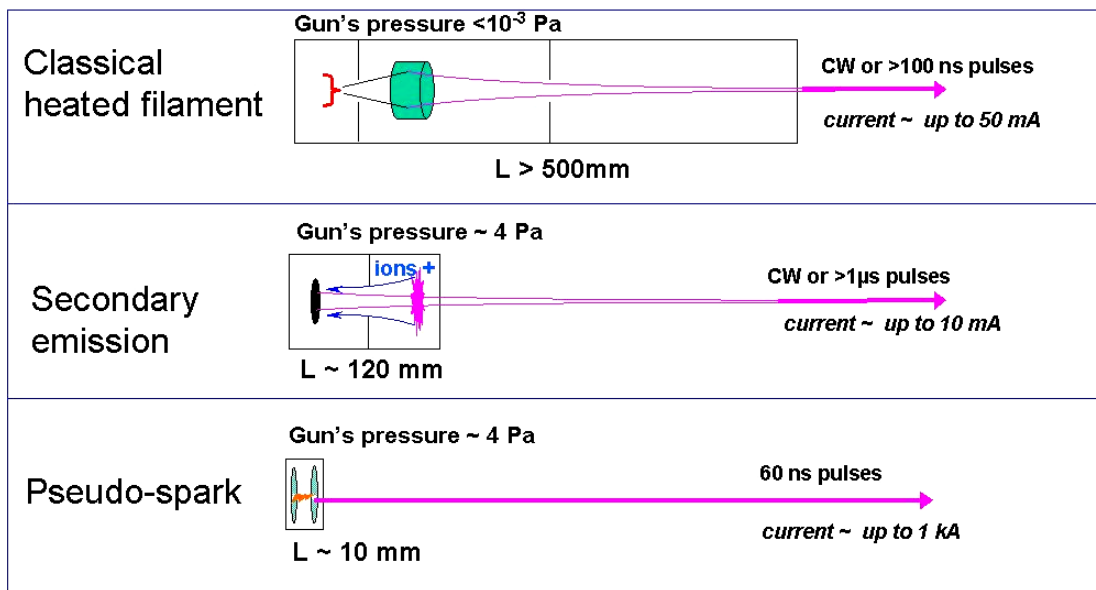
Figure 16 - The three main types of electron guns

Gun	Measurement duration	Repetition rate	Measurements
Classical gun (filament-heated) (beam 30 kV, 1 mA, diam 1 mm)	100 ns to CW	CW or pulsed up to 10 MHz	All EBF measurements in low enthalpy conditions (Hi/RTa < 10)
Pseudo-spark (beam 60 kV, 100 A, diam 0.1 mm)	30 ns à 5 µs	pulsed up to 1 kHz	Velocity in all conditions; sufficiently miniature to be placed inside a body in the flow
Secondary emission (25 kV, 10 mA, diam 1 mm)	1µs to CW	CW or pulsed up to few kHz	All EBF measurements

Table 3 – Main properties and performances of different types of electron gun

Usually heated filament or pseudo-spark electron guns are used to generate the electron beam in windtunnels. But these devices are quite difficult to be used in a flight experiment because of their mass, their consumption and the secondary vacuum which is required for their operation.

2.5 EBF for inflight measurements

ONERA has developed in the frame of one of its internal project on hypersonics, a new concept of gun that associates small size, low power consumption and that does not require secondary vacuum to operate. These features are expected to greatly ease the in-flight application of EBF. The prototype of such a gun is illustrated on Figure 17. Ions produced through an electrical discharge between the anode (wire) and the walls are accelerated towards the cathode maintained at a high voltage (- 20 keV). Their impacts against the cathode extract electrons which are accelerated counter-wise and are collimated into a thin beam by the geometry of the system. Operation with internal pressure up to 5 Pa has been demonstrated.
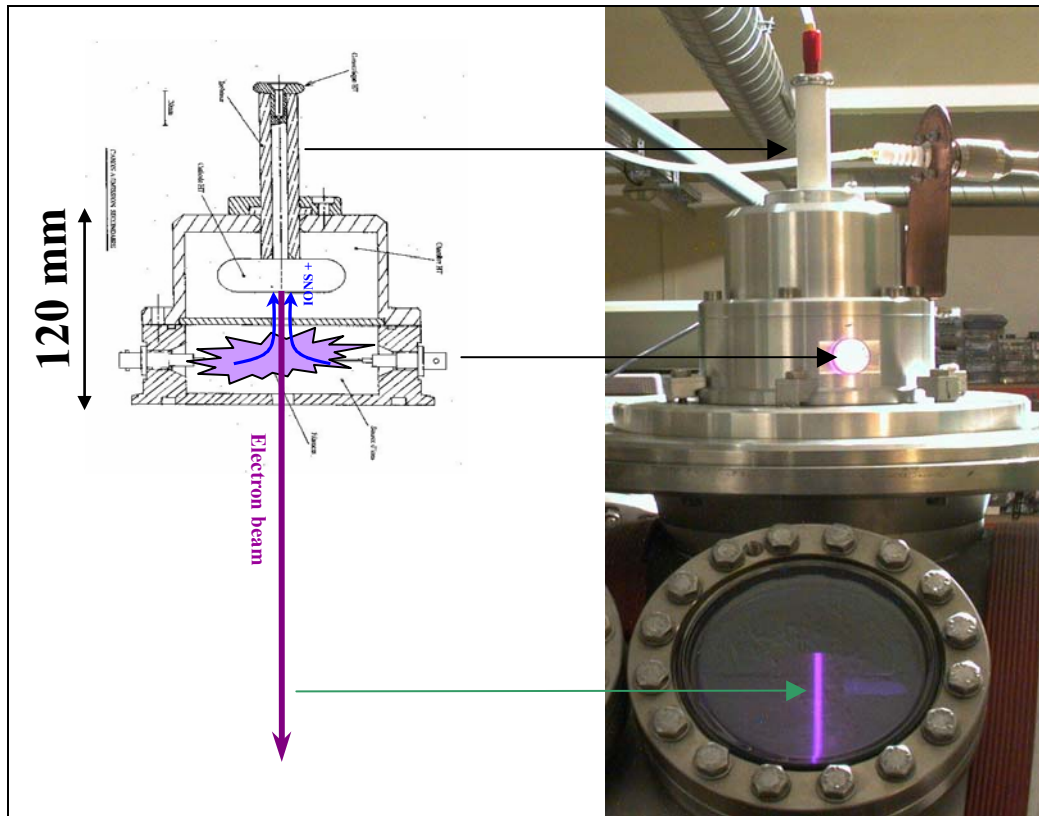
Figure 17 - Miniature electron gun prototype

The other main characteristics of this secondary emission electron gun (SEEG) are:

- 30 kV acceleration voltage
- 1 mA beam current
- 2-3 Pa internal pressure
    A single stage differential pumping with a small turbopump (10 l/s) and a 3 mm conductance is able to maintain less than 3 Pa in the gun with more than 100 Pa outside (Figure **18**).
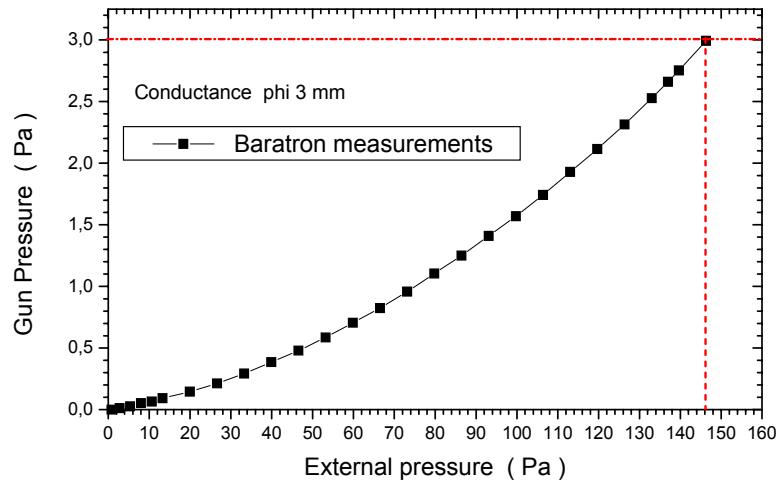
Figure 18- Internal gun pressure versus external pressure

A feasibility study to use such a gun for in-flight measurements on board an atmospheric re-entry has been recently performed for the ESA-EXPERT demonstration vehicle [18] and we give below the main outcome of this study.

The primary objectives of an EBF payload envisioned onboard a re-entry vehicle is to provide the following measurements with a spatial resolution in the order of a few mm3:

- N_2 density: $\rho/(\rho\infty(N_2))$ profile across the shock layer using CCD

- Temperatures of rotation and vibration of N_2 using medium and resolution spectrometers,

- NO density at one or several points in the shock layer using the spectrometer for Tv or a CCD camera with an optical filter cantered on one of the g bands in the UV spectral domain.

An example of proposed set up aboard the ESA EXPERT vehicle project is depicted in Figure 19. The measurements are to be performed along a line perpendicular to the wall at about one third of the vehicle length starting from the nose of the vehicle. The shock layer thickness along the measurement line is about 200 mm for Mach numbers over 10 as illustrated in Figure 20 which presents also some other CFD calculated expected conditions which are pertinent to EBF. The position of the setup is dictated by a location on the surface where an optical window can resist the high heat loads.

The measurements are to be provided at a minimum repetition rate of 10 Hz between the altitudes 70 km to 50 km.
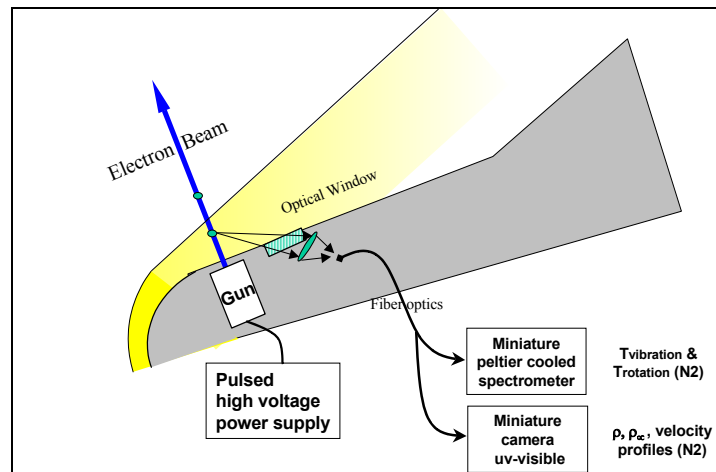
Figure 19 - EBF measurements envisioned on board the EXPERT demonstrator
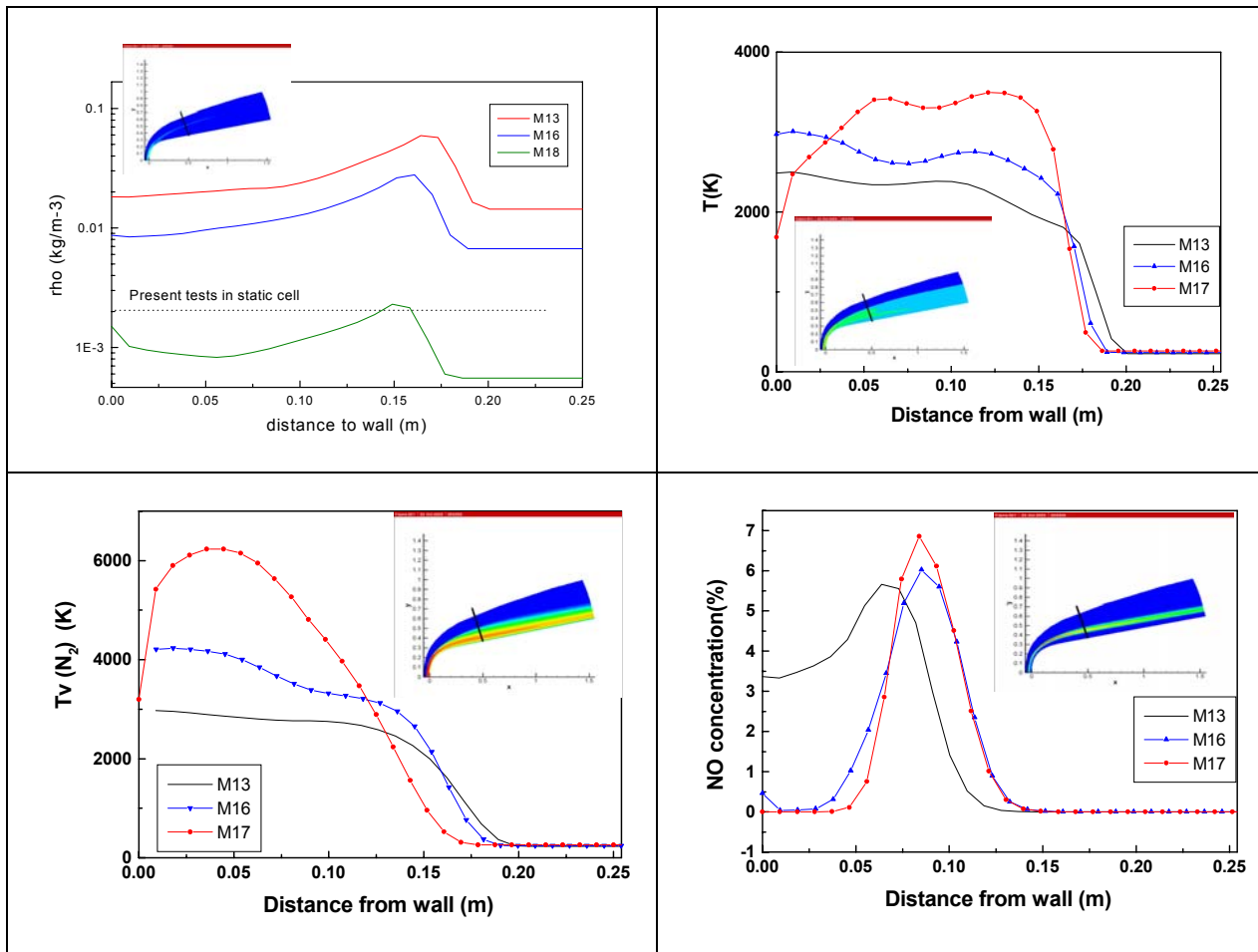
Figure 20 - Expected values of the parameters targeted by EBF for Expert[18]

A preliminary layout of the EBF payload in the EXPERT vehicle is illustrated in Figure 21. It has been optimized to take into account the following requirements:

- Flat surface for the optical window

- The optical axis for fluorescence detection has been tilted so as to intersect the electron beam at the minimum distance of 200 mm from the surface in order to visualize part of the shock layer (for Tvib and NO) and also part of the upstream flow (for upstream density measurements).
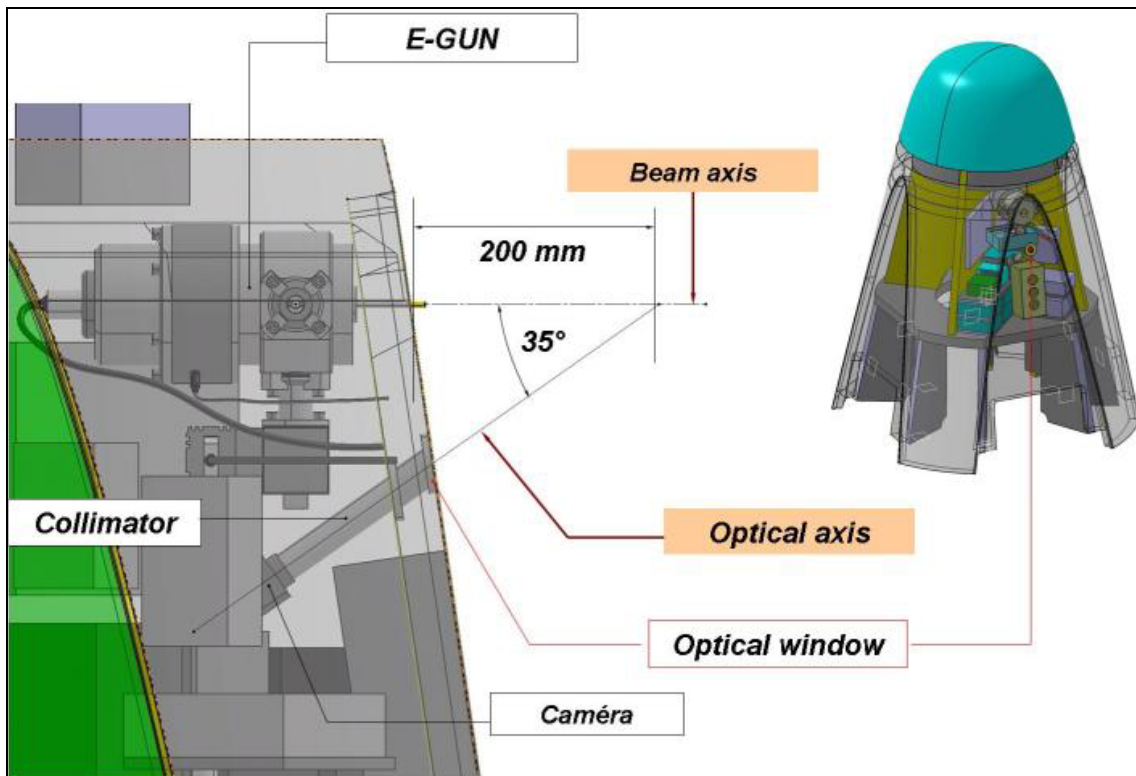
Figure 21 - Payload EBF preliminary layout

The power budget is about 60 W and the data rate is at 1Mbps.

However the feasibility study showed that the envisioned setup is not quite ripe and further studies are required to reduce the complexity of the setup.

3   RAYLEIGH Lidar for Density Measurements

Past re-entry demonstration flights have shown that atmospheric density ρ_∞ is a key input parameter which must be known with an accuracy of a few percent in order to evaluate correctly the flight dynamics and aerothermal heating from high altitudes high Mach numbers flight data [19]. This accuracy cannot be attained with actual classical barometric measurement system and it is not realistic either to rely on standard atmosphere models as there can be unpredictable departures from these models which may reach extremes as large as 80% (3σ) over vertical distances of less than 1 km.

A lidar based on Rayleigh scattering is one the most promising optical techniques which can provide in-flight measurement of the atmospheric density around a re-entry vehicle with accuracy close to 1 % for the altitude range from 40 to 80 km. Moreover, the measured value is independent of other flight or atmosphere data. Lidar in space is not new and there are already a few examples which have successfully operated aboard satellites during the last two decades for earth atmosphere probing [20][21][22]. An experiment aboard a rocket has also been successfully tried for atmospheric density measurement during the ascent phase [23].

In the frame of an internal project dedicated to identify and develop advanced diagnostics aboard re-entry vehicles and through CNES support, ONERA is developing a short range Rayleigh Lidar for in flight measurements of local atmospheric density at a few meters distance around a re-entry demonstrator vehicle. Figure 22 shows the generic features of a potential setup aboard the CNES pre-X vehicle[25].
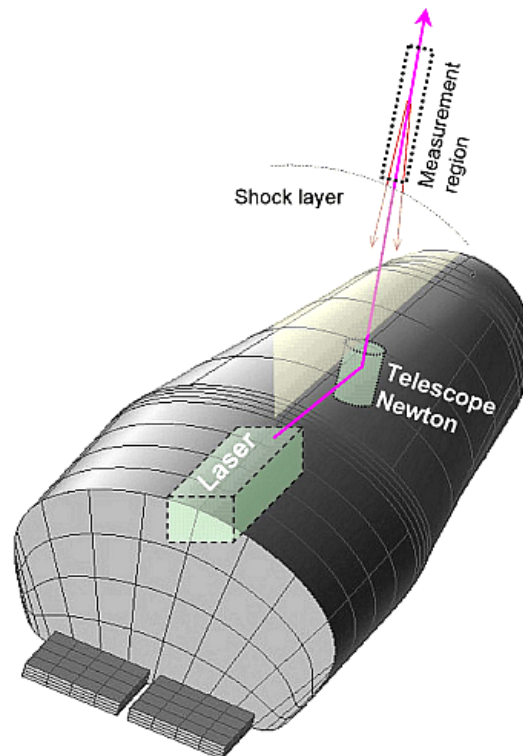
Figure 22 - Potential setup for a Rayleigh Lidar aboard the pre-X vehicle (courtesy CNES)

Figure 23 depicts the expected atmospheric conditions to be encountered along the pre-X reentry path. These conditions are used to design the Lidar instrument for atmospheric density measurements in altitude range 40 to 80 km with optimized performance around 60 km where the peak heat flux is expected to

occur on the vehicle.
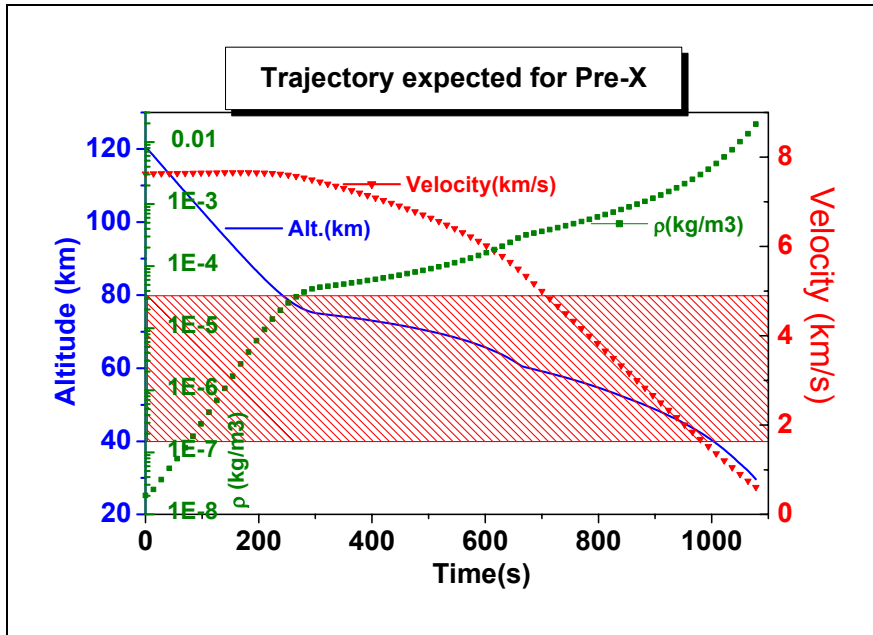
Figure 23 - Some atmospheric conditions expected along the pre-X trajectory

3.1 Rayleigh Lidar Principle

The inelastic interactions of an electromagnetic wave with a molecule induce a dipole moment in the molecule which then emit radiation at the same frequency as the exciting radiation.
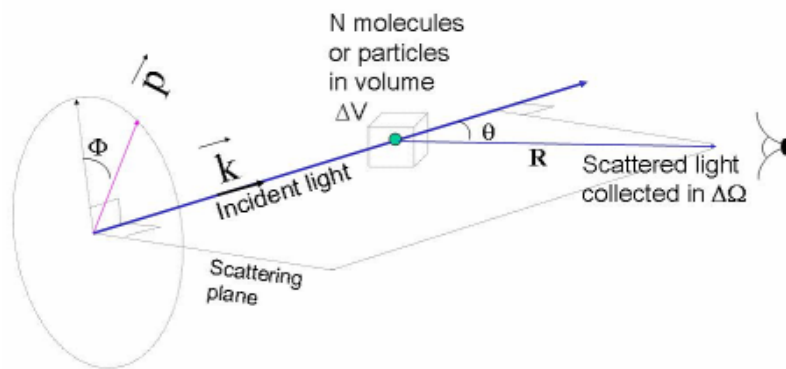
Figure 24 – Light scattering parameters definition

From notations in Figure 24, the intensity I_d of the scattered light at angle θ from the incident light direction is given for a single molecule or particle by the expression:

$$I_d = I_0 \int_{\Delta\Omega} \frac{\partial\sigma}{\partial\Omega}\Big|_{\theta,\Phi,\lambda,x} d\Omega \quad (1)$$

where

- I_0 is the intensity of the incident light

- $\Delta\Omega$ is the solid angle of light collection $\sim A/R^2$

    with A the surface area of light collection and R the distance between scatterer and detector

- $\dfrac{\partial\sigma}{\partial\Omega}\Big|_{\theta,\Phi,\lambda,x}$ is the cross-section of scattering at the angles defined in Figure 24, at wavelength λ and depending on other parameters denoted x here and which will be developed if needed afterwards.

For a molecule, the Rayleigh differential cross section can be expressed as

$$\frac{\partial\sigma}{\partial\Omega}\Big|_{\theta,\Phi,\lambda,x} = \sigma_{\lambda,x}(\cos^2\Phi\cos^2\theta + \sin^2\Phi) \quad (2)$$

where the total Rayleigh cross section can be further expressed [24] as

$$\sigma_\lambda = \frac{24\pi^3}{N_s^2\lambda^4}\frac{(n_\lambda^2 - 1)^2}{(n_\lambda^2 + 2)^2}F_\lambda \quad (3)$$

where N_s is the molecular number density ($12.54743 \ 10^{19} \ \text{cm}^{-3}$) for standard air, n_λ is the refractive index and F_λ is the King correction factor which takes into account the anisotropy of non-spherical molecules. Figure 25 presents the total Rayleigh cross sections from reference [24] for air molecules at standard atmospheric conditions and it is customary to use also these values at high altitudes in absence of more accurate data.
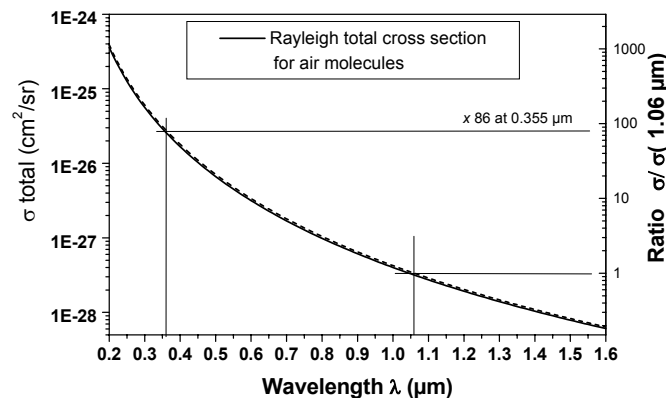
Figure 25 - Rayleigh cross section as a function of wavelength (from [24])

For circularly and unpolarized light, the observed differential cross section at angle θ is obtained by averaging over all possible polarizations Φ. Since the average of $\cos^2\Phi$ and $\sin^2\Phi$ are both ½, the differential scattering cross section for molecular scattering becomes proportional to the well known dependency $1+\cos^2\theta$ for sunlight scattering in the atmosphere. However, if the light is linearly polarized (as in some lasers) such that the direction is perpendicular or parallel to the scattering plane it is possible to minimize or maximize the angular dependence of the differential cross.

In our case, we will be in a situation where the laser source is polarised with Φ=0 and in a backscattering geometry with θ close to π . With the help of equations 1 to 3 and associated terms, one can derive the Lidar equation which we will report here from reference [23] :

$$I_d(z) = T_L I_0 . N(z) . A . \sigma_\lambda . \int_{r1}^{r2} \frac{T_g^{\,2}(r)\,dr}{r^2}$$

- N(z) is the density of scatterers per unit volume at altitude z,

- r = distance detector and unit volume of the laser beam,

- r1 and r2 : limits of the laser beam observed by the detector,

- T_g is the transmission factor to take into account any absorption of the laser intensity in the flow before reaching the scattering volume and absorption of the Rayleigh scattered light on its path to the detector (~1 in our case),

- T_L is the transmission coefficient for all optical elements (emission and detection) of the Lidar system .

3.2 Feasibility of Rayleigh Lidar for vehicle like pre-X

The Lidar envisioned is a short range one to measure the atmospheric density at about 2 m from the vehicle outside the shock layer (Figure 22).

3.2.1 Laser requirements

The following criteria have been studied to choose the laser wavelength :
1) Rayleigh scattering efficiency v/s wavelength
2) Available wavelengths for rugged lasers
3) Sun rays scattering on the higher atmosphere layers
4) Shock layer radiation
5) Black body radiation for hot structures around the optical window

The three last aspects bringing background light disturbances to the measurements are illustrated in Figure 26.
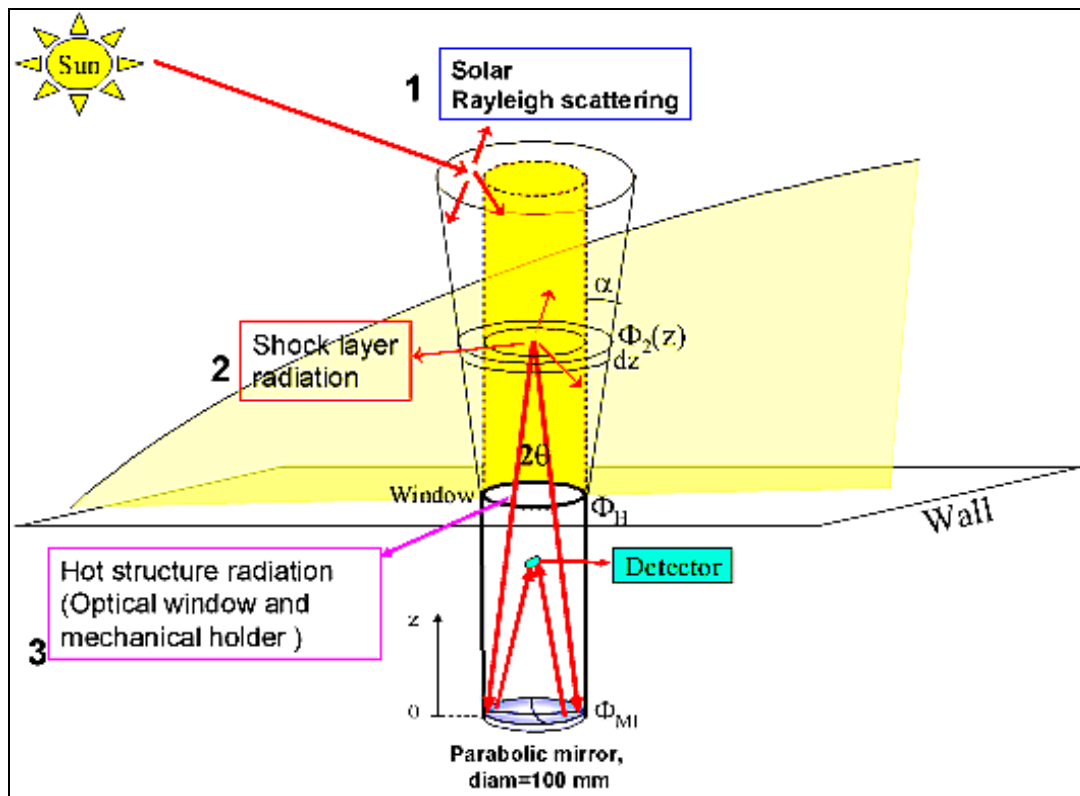
Figure 26 - Expected sources of background light

The evaluation of the factors influencing the choice of the laser wavelength is presented in Figure 27. All curves are normalized to their values corresponding to the reference wavelength value of 1.06 μm (for the base emission wavelength of a YAG laser). The calculations are performed for a pulsed detection scheme with short integration times (~100 ns) in the aim to diminish background radiation. In our case, the hot optical window system and indirect scattering from sun rays have lower influence than shock layer radiation and Rayleigh wavelength efficiency.

The outcome of this evaluation limits our choice of laser wavelength to the spectral region from 300 to 400 nm where calculations predict that shock layer radiation intensity seems to be one decade less and where Rayleigh scattering is about 30 times more intense than at 1.06μm. For the last criterion, the product of laser wavelength (λ) times Rayleigh cross-section ($1/\lambda^4$ dependency) is the relevant parameter for proper evaluation of scattering efficiency [23]. For further calculations below, we will take the wavelength value of 355 nm corresponding to a frequency tripled YAG or Ytterbium fiber laser which are now quite common lasers and which have in flight perspectives.
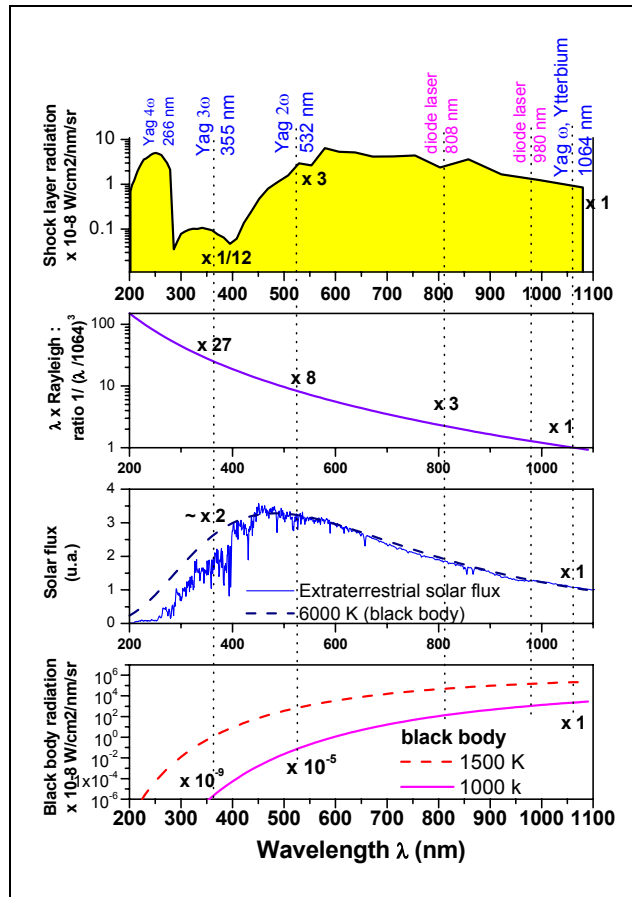
Figure 27 - Main criteria for laser wavelength

A pulsed laser (~30 ns pulses) coupled to short openings (< 100 ns) of the optical detection system have to be used in order to diminish background radiation contribution to the overall optical signal. Calculations of the laser power needed to perform density measurements at a distance farther than 2 m from the vehicle with an accuracy of 1 % with an ideal photon counting system lead to a minimum laser pulse energy of 20 mJ at 355 nm. This energy can be through a single pulse or through an accumulation of pulses of lower energies.

Another requirement for the laser is an adequate frequency to allow a spatial resolution of a few meters particularly around the 60 km altitude. From data in Figure 23, a measurement frequency around 20 Hz satisfies this requirement as illustrated in Figure 28. This is compatible to available YAG lasers (20 mJ at 20 Hz at 355 nm) or fiber lasers (0.02 mJ at 20 kHz at 355 nm). In the last case, accumulation on 1000 pulses has to be performed to attain the 20 mJ necessary for one measurement point.
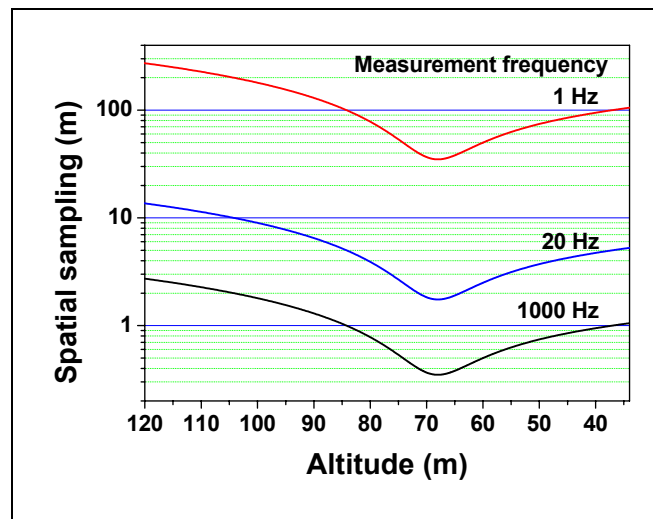
Figure 28 - Spatial sampling at different measurement frequencies

A trade-off study on available lasers which have the power and wavelength requirements of 20 mJ at 20 Hz at 355 nm as discussed above and which are of small dimensions lead to the following three types:

- Frequency -tripled YAG (355 nm)

- Frequency -tripled Ytterbium fiber laser (355 nm)

- Excimer laser (351 nm)

The last possibility has to be discarded because the actual technology provides a too complex system for in flight operation. Of the first two possibilities left, YAG technology is more well mastered but the wall-plug energy efficiency is yet too low : laboratory lasers show that at least 1 kW electrical power is required for operation in our case. Such an amount of power presently seems to be prohibitive for its use on a small demonstrator vehicle like the pre-X. The recent developments in fiber laser technology offer a promising solution as less than 300W electrical power is required for our application. Furthermore, such a laser is quite miniature and robust, which will greatly facilitate its use for flight operation. It can operate in a pulsed regime but at quite high frequency (20 kHz). The main difficulty for our needs resides in the frequency conversion to UV, in the pulsed regime, from the natural laser emission in these fibers which occur in near infrared domain at 1.06 μm or 1.55 μm. Figure 29 presents the UV conversion scheme needed in our case. For this conversion, a fixed polarization is needed and up to now this is quite difficult to obtain for high energy pulsed fiber lasers. Fortunately, this critical aspect is being intensively studied by several laser manufacturers and different solutions have been found (ex : non-circular symmetry fibers,..).
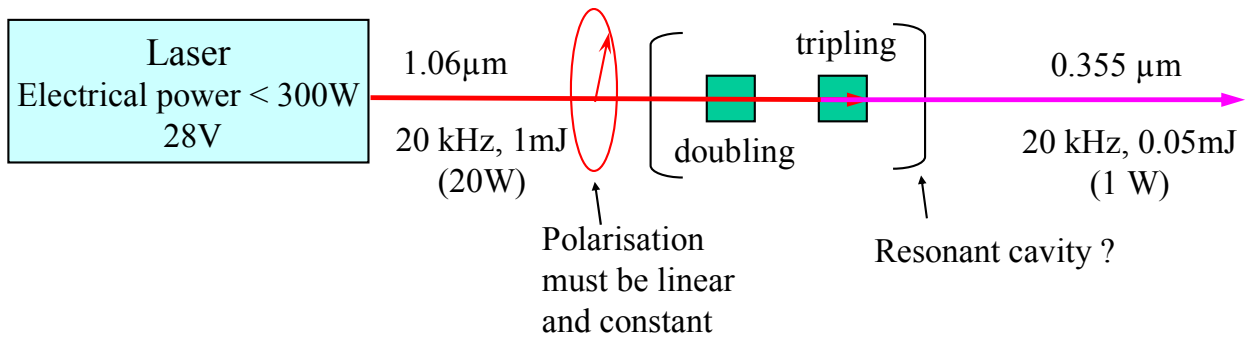
Figure 29 - Laser frequency conversion to UV

3.2.2 Optical window on vehicle wall

We must mention here that an in-flight Lidar requires the presence of an optical window of quite large diameter (~100 mm) on the wall of a reentry vehicle which have quite high surface temperatures. There is therefore a requirement for studies on high temperature materials for optical windows and their insertion in a thermal protection system as well as on radiation from the shock layer or other high temperature elements that can bring perturbations to the optical detection. These aspects are illustrated in Figure 30.
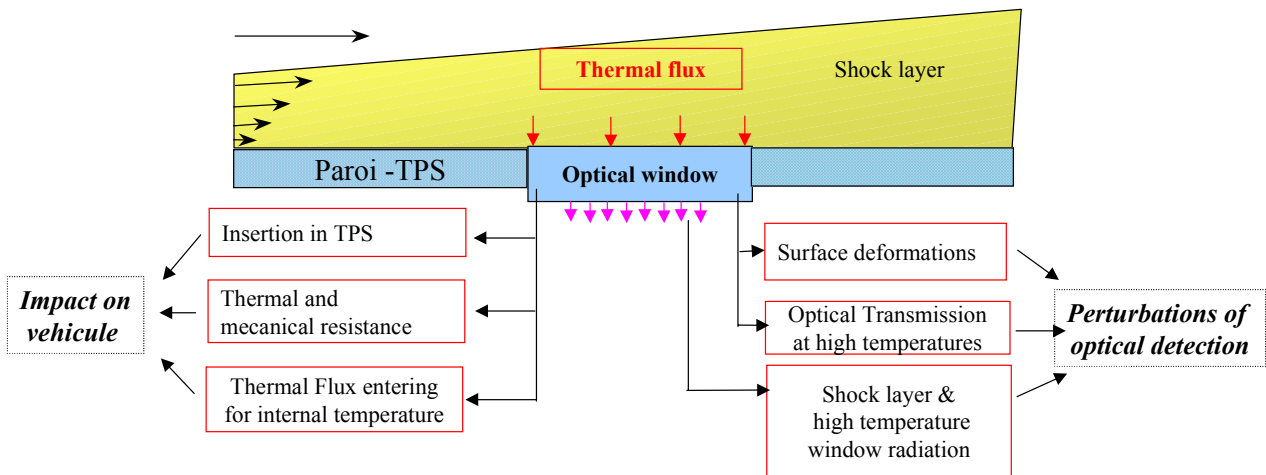
Figure 30 – Some optical interface issues

4   References

[1]   GRUN A. E., SHOPPER E., SCHUMACHER B., "Electron Shadowgraph and Afterglow Pictures of Gas Jets at Low Densities", J. Appl. Phys., 24, p1527, 1953

[2]   MUNTZ E. P., "The Electron Beam Fluorescence Technique", AGARDograph 132, 1968

[3]   MOHAMED A., "EBF in blow-down hypersonic wind tunnels', Phd Dissertation, Paris XI, 1991

[4]   COLOMBA R.;BONNET J. 'Canon à électrons pour technique FFE en nappe', ONERA RT 46/3409 PN, 1994

[5]   Weaver D. P., Wadsworth D.C., Campell D., Muntz E.P., *DSMC Comparison with Electron Beam Measurements of Sonic Orifice Expansion Flow of Nitrogen ,* Proceedings of the 18th International Symposium on Rarefied Gas Dynamics, Vancouver, Canada, AIAA, Washington, DC, Vol.158, pp.1314 (1994)

[6]   Mohamed A.K., Pot T., Chanetz B., Diagnostics by Electron Beam Fluorescence in Hypersonics,ICIASF'95 Record 95-CH3482-7,14.1, International Congress on Instrumentation in Aerospace Simulation Facilities, Wright-Patterson AFB, Ohio, USA, July 1995

[7]   Gochberg, L. A., "Electron Beam Fluorescence Methods in Hypersonic Aerothermodynamics", Prog. Aerospace Sci., Vol. 33, 1997, pp. 431-480.

[8]   Larigaldie, S., Bize, D., Mohamed, A. K., Ory, M., Soutadé, J., and Taran, J. P., *Velocity Measurement in High Enthalpy, Hypersonic Flows Using an Electron-Beam-Assisted Glow Discharge*, AIAA Journal, Vol 36, No 6, (1998)

[9]   LENGRAND J-C., "Mesure des températures de rotation dans l'azote à basse densité par la sonde à faisceau électronique. Application à l'étude d'écoulements.", Thèse de Doctorat en Sciences Physiques, Université Paris VI, 1974

[10] Gundlach G., Dankert C., *Rotational Accommodation of NO on a Hot SiC-Surface in a Rarefied Flow,* Proceedings of the 18th International Symposium on Rarefied Gas Dynamics, Vancouver, Canada, AIAA, Washington, DC, Vol.158, pp.976 (1994)

[11] S. Novopashin, C. Dankert, K. Lehmköster, A.Mohamed, T. Pot, Rotational Temperatures of N2-molecules Reflected from a Wall, Rarefied Gas Dynamics, Proceedings of the 20th International Symposium, 19-23 August 1996, Beijing/China, Ed. Ching Shen, Peking University Press, Beijing, China, 1997

[12] De Leeuw J.H., Davies W.E.R., Measurement of temperature and density in the upper atmosphere using an electron beam, Can. j. Phys, 50(10), 1044 (1972)

[13] O'Neil R.R., Pendelton W.R., Hart A.M., Stair A.T., Vibrational temperature and molecular density of nitrogen measured by rocket-borne electron beam induced luminescence, J. Geophy. Res., 79(13),

1942, (1974)

[14] Cattolica R.J., Schmitt R.J., Palmer R.E., Feasibility of non-intrusive optical diagnostic measurements in hypersonic boundary layers for flight experiments, AIAA paper 90-0627 (1990)

[15] Kawashima T., Oyama K. and Suzuki K., A Measurement of Vibrational-Rotational Temperature and Density of Molecular Nitrogen in the Upper Atmosphere by Rocket-Borne Electron Beam Induced Luminescence, The Institute of Space and Astronautical Science(Japan), report n° 672, 1999

[16] Christiansen, J., and Schultheiss, C., *Production of High Current Particle Beams by Low Pressure Spark Discharges*, Z. Physik, Vol. A290, pp. 35-41 (1979)

[17] Larigaldie, S., *Study of the Breakdown Phase in a Pseudospark Switch: Part I-Basis Experiments and Crude Model, Part II-Ultrafast CCD Cameragrams Using HE$^+$ Spectral Line Emission*, IEEE Trans. on Plasma Science, Special Issue on Physics and Application of Pseudospark Discharges,Vol. 23, No. 3, pp 362-374 (1995)

[18] L. Walpot, H. Ottens, " FESART/EXPERT Aerodynamic and Aerothermodynamic Analysis of the REV and KHEOPS Configurations", TOS-MPA/2718/LW, 16 September 2002

[19] Macret J.L., Leveugle T., "The ARD (Atmospheric Reentry Demonstrator) Program: an overview", AIAA Paper 99-4934, 1999

[20] D. M. Winker, R. H. Couch, and M. P. McCormick, "An overview of LITE: NASA's Lidar In-space Technology Experiment," Proc. IEEE 84, 164–180 (1996).

[21] M.-L. Chanin, A. Hauchecorne, C. Malique, M. Desbois, G. Tulinov, and V. Melnikov, "The ALISSA lidar on board the MIR platform," in Advances in Laser Remote Sensing, A. Dabas,C. Loth, and J. Pelon, (pp. 23–26) in Edition de l'Ecole Polytechnique, Palaiseau, France (2001)

[22] http://glas.gsfc.nasa.gov/ : GLAS (the Geoscience Laser Altimeter System) is the first laser-ranging (lidar) instrument for continuous global observations of Earth. From aboard the Ice Cloud and Elevation Satellite (ICESat) spacecraft launched on January 12, 2003.

[23] Torkild Eriksen, Ulf-Peter Hoppe, Eivind V. Thrane, and Tom A. Blix, "Rocketborne Rayleigh Lidar for in situ measurements of neutral atmospheric density", APPLIED OPTICS, Vol. 38, No. 12, 20 April 1999.

[24] BUCHOLTZ Anthony, "Rayleigh-scattering calculations for the terrestrial atmosphere", APPLIED OPTICS, Vol. 34, No. 15,p2765, 20May 1995

[25] Guedron, S.; Devezeaux, D, "Need of Pre-X Reentry Experimental Vehicle for ATD Phenomena Mastering", 4th European Symposium on Aerothermodynamics for Space Vehicles, Capua, Italy, October 2001.